Balazs Varszegi
Department of Applied Mechanics,
Budapest University of Technology
and Economics,
MTA-BME Lendulet Human
Balancing Research Group,
Budapest H-1111, Hungary
e-mail: varszegi@mm.bme.hu

Denes Takacs
MTA-BME Research Group on
Dynamics of Machines and Vehicles,
Budapest H-1111, Hungary
e-mail: takacs@mm.bme.hu

Gabor Stepan
Department of Applied Mechanics,
Budapest University of Technology
and Economics,
Budapest H-1111, Hungary
e-mail: stepan@mm.bme.hu

Stability of Damped Skateboards Under Human Control

A simple mechanical model of the skateboard–skater system is analyzed, in which a linear proportional-derivative (PD) controller with delay is included to mimic the effect of human control. The equations of motion of the nonholonomic system are derived with the help of the Gibbs–Appell method. The linear stability analysis of the rectilinear motion is carried out analytically in closed form. It is shown that how the control gains have to be varied with respect to the speed of the skateboard in order to stabilize the uniform motion. The critical reflex delay of the skater is determined as functions of the speed, position of the skater on the board, and damping of the skateboard suspension system. Based on these, an explanation is given for the experimentally observed dynamic behavior of the skateboard–skater system at high speed. [DOI: 10.1115/1.4036482]

Keywords: nonholonomic mechanics, skateboard, human balancing, time delay

1 Introduction

The first skateboard was invented a century ago to carry surfboards to the ocean easier, namely, simple metal wheels were installed to wooden boards. The present configuration of the wheel suspension became common later only, by which, the wheel-pairs turn around their steering axes if the skateboard is tilted around its longitudinal axis. Due to this mechanism that provides specific kinematic constraints, the understanding of the motion of the skateboard is a challenging task. The equations of motion of the resulted nonholonomic system can be derived by means of Kane's method [1], which was applied in the first scientific publication in this area [2]. Hubbard investigated the linear stability of the skateboard, and he realized the positive effect of the speed, e.g., the higher the speed is, the more stable the skateboard is.

The speed-dependent stability of nonholonomic systems still has unexplored dynamic phenomena although they have been investigated for more than 100 yr. This is clearly shown by recent publications, where the lateral stability of the bicycle and the three-dimensional biped walking machines was studied (see, for example, Refs. [3] and [4]). For nonholonomic systems, the investigation of the stability of skateboards was made in the 1990s and in the new millennium. Nonlinear analysis was carried out [5], and controlled motions were also investigated [6].

The other interesting challenge in connection with the skateboard–skater system is to explain the balancing effort of the skater on the skateboard. There are publications where the human control was taken into account [7,8], but the reflex delay of the skater was considered in Refs. [9] and [10] only. Nevertheless, the importance of the reflex delay has been shown by many papers for human balancing models from both biological and engineering points of view [11–15].

In this paper, a mechanical model of the skateboard is constructed in which human control is taken into account. A typical modeling approach is used to present the human control efforts, namely, the skater's control adjusts the mass center of his body by a torque at his ankle. A linear PD controller is applied to the control loop, in which we also consider the reflex delay. Similar models were used in Refs. [12] and [15] although some other control models can present more realistic higher-frequency behavior (for example, see McRuer's approach in Ref. [16]).

In order to obtain the equations of motion in the most compact form that supports the analytical investigation the best, the Appellian approach [17] is used instead of the classical Lagrangian one [8]. The stability analysis of the rectilinear motion is investigated via closed form calculations. Criterion is given for the time delay, meanwhile the effects of the skater's longitudinal position and the stiffness/damping parameters of the suspension system are also in focus.

2 Mechanical Model

The mechanical model in Fig. 1 is based on Ref. [9] but here the suspension of the board also contains an additional torsional damper. The model consists of two massless rods connected by a hinge at point S. One of the rods represents the board between the points F (front) and R (rear), while the other rod stands for the skater between the points S and C (center of gravity). The lumped

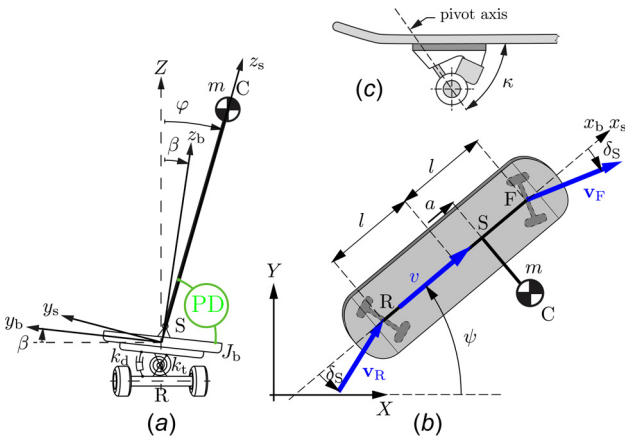

Fig. 1 Mechanical model of the skateboard–skater system [9]; panel (*a*) shows the back view of the mechanical model, panel (*b*) shows the top one and panel (*c*) shows the skateboard suspension system

Contributed by the Design Engineering Division of ASME for publication in the JOURNAL OF COMPUTATIONAL AND NONLINEAR DYNAMICS. Manuscript received September 21, 2016; final manuscript received March 20, 2017; published online May 4, 2017. Assoc. Editor: Bernard Brogliato.

mass m represents the mass of the skater at the free end of the vertical rod.

Although the board is assumed massless, the mass moment of inertia of the board is kept and represented by $\mathbf{J}_b$ with respect to the center of the board. Due to the symmetry of the board, the inertia around its longitudinal, lateral, and vertical axes are denoted by J_1, J_2, and J_3, respectively.

The remaining parameters of the model are the following: $2h$ denotes the height of the skater, $2l$ is the length of the board, a indicates the longitudinal location of the skater on the board ($a>0$ means that the skater stands ahead of the center of the board), and g stands for the gravitational acceleration.

The loss of contact between the ground and the wheels is not considered, so the longitudinal axis of the board is always parallel to the ground. Therefore, five generalized coordinates can describe the motion uniquely: x and y are the coordinates of point S; ψ describes the longitudinal direction of the board, and φ and β are the deflection angles of the skater and the board relative to the vertical direction, respectively (see Fig. 1).

In order to investigate the skater–board interaction analytically, the control effort of the skater is taken into account in the simplest possible way. Accordingly, most of the balancing movements (like bending the spine, swinging the arms) are neglected except the ankle torque [2,5–8,10]. This model is widely used for stability analysis, since the small body angles in human balancing are corrected via ankle torque, while the hip or arm motions are used at large body angles only.

Consequently, the resulting model is analogous to the simplest human balancing models, which include active (controlled) and passive (uncontrolled) torques at the ankle [13,14,18–20]. Here, only the active one is investigated, while the muscle stiffness and damping originated in the muscle stretching related to the ankle rotation are neglected. The active torque arises from muscle activation due to the delayed neuromuscular sensory feedback from the proprioceptive, vestibular, and visual systems. We take into account only the last two sensory systems. The vestibular and visual ones provide information about the absolute body angle (φ) with respect to the vertical direction and the angular velocity ($\dot{\varphi}$), the corrective torque according to them is determined in our model by a linear time-delayed PD controller [12]

$$M_{\mathrm{PD}} = p\varphi(t-\tau) + d\dot{\varphi}(t-\tau) \tag{1}$$

where τ refers to the time delay, and p and d represent the proportional and the derivative control gains, respectively.

As one can see in Fig. 1, the free rotation of the board about its longitudinal axis is obstructed by a torsional spring of stiffness k_t and by a torsional damper of damping coefficient k_d beside of the control torque produced by the skater. These dynamical elements of the system are originated in the special wheel suspension system of the skateboard.

We consider that the wheels of the skateboard roll perfectly for small steering angles. By means of the geometry of the suspension system, the direction of the velocities $\mathbf{v}_F$ and $\mathbf{v}_R$ of the points F and R can be expressed in terms of the generalized coordinates (see Refs. [2] and [7]). Namely, a nonlinear connection arises between the steering angle δ_S and deflection angle of the board β (see Refs. [21] and [22] and further details in Ref. [2] on the functioning of the skateboard's suspension system)

$$\sin\beta\tan\kappa = \tan\delta_S \tag{2}$$

where κ is the constant angle in the suspension system between the pivot axis and the board as it is shown in Fig. 1(*c*). Based on these, two scalar kinematic constraining equations can be constructed

$$(\cos\psi\sin\beta\tan\kappa - \sin\psi)\dot{x} + (\sin\psi\sin\beta\tan\kappa + \cos\psi)\dot{y} + (l-a)\dot{\psi} = 0 \tag{3}$$

$$(\cos\psi\sin\beta\tan\kappa + \sin\psi)\dot{x} + (\sin\psi\sin\beta\tan\kappa - \cos\psi)\dot{y} + (l+a)\dot{\psi} = 0 \tag{4}$$

A third kinematic constraint is also introduced in the model: the prescribed longitudinal speed v of the board is constant in time

$$\dot{x}\cos\psi + \dot{y}\sin\psi = v \tag{5}$$

It can be proved that the presence of this third kinematic constraint does not modify the linear stability of the rectilinear motion.

3 Mathematical Model

The derivation of the equations of motion can be carried out by means of the Gibbs–Appell method [17]. This method is efficient in the sense that it provides the equations in a first-order compact form. This method requires linear kinematic constraints in terms of generalized velocities. Since this criterion is satisfied by Eqs. (3)–(5), the Gibbs–Appell equations can be obtained in the form of

$$\frac{\partial \mathcal{A}}{\partial \dot{\sigma}_i} = \Gamma_i, \quad i = 1,2 \tag{6}$$

where $\mathcal{A}$ is the so-called energy of acceleration what is differentiated with respect to the so-called pseudo-acceleration $\dot{\sigma}_i$. The right-hand side is the so-called pseudoforce Γ_i.

The pseudovelocities σ_i can be chosen intuitively, by which the kinematic constraint forces can be eliminated. In our case, two pseudovelocities are needed since the difference between the numbers of the generalized coordinates and the kinematic constraints is two. An appropriate choice can be the angular velocity components σ_1 and σ_2 of the skater and the skateboard around the longitudinal axis, respectively,

$$\sigma_1(t) := \dot{\varphi}(t) \quad \text{and} \quad \sigma_2(t) := \dot{\beta}(t) \tag{7}$$

This choice is appropriate since the system of equations, which consists of the kinematic constraining Eqs. (3)–(5) and the definitions (7) of the pseudovelocities, can be solved uniquely for the generalized velocities

$$\begin{bmatrix} \dot{x} \\ \dot{y} \\ \dot{\psi} \\ \dot{\varphi} \\ \dot{\beta} \end{bmatrix} = \begin{bmatrix} v\left(\cos\psi + \dfrac{a}{l}\tan\kappa\sin\beta\sin\psi\right) \\ v\left(\sin\psi - \dfrac{a}{l}\tan\kappa\sin\beta\cos\psi\right) \\ -\dfrac{v}{l}\tan\kappa\sin\beta \\ \sigma_1 \\ \sigma_2 \end{bmatrix} \tag{8}$$

The derivation of both sides of this expression with respect to time leads to the generalized accelerations, as functions of the pseudo-acceleration, pseudovelocities, and generalized coordinates.

In case of our model, the acceleration energy $\mathcal{A}$ reads

$$\mathcal{A} = \frac{1}{2}m\,\mathbf{a}_C\cdot\mathbf{a}_C + \frac{1}{2}\boldsymbol{\alpha}^T\mathbf{J}_b\boldsymbol{\alpha} + \boldsymbol{\alpha}^T(\boldsymbol{\omega}\times(\mathbf{J}_b\boldsymbol{\omega})) + \frac{1}{2}\boldsymbol{\omega}^T(\mathbf{J}_b\boldsymbol{\omega})\omega^2 \tag{9}$$

The first term in this formula refers to the skater modeled with a lumped mass, while the other terms refer to the board that has negligible mass but it has finite mass moment of inertia. In Eq. (9), we have

$$\mathbf{a}_C \cdot \mathbf{a}_C = 2\frac{v\tan\kappa}{l^2}(v\sin\beta(l - h\tan\kappa\sin\beta\sin\varphi) + al\sigma_2\cos\beta) \times h\dot{\sigma}_1\cos\varphi + h^2\dot{\sigma}_1^2 + \cdots \tag{10}$$

which are necessary parts of the square of the lumped mass' acceleration

$$\underset{(x_b,y_b,z_b)}{\boldsymbol{\omega}} = \begin{bmatrix} \sigma_2 \\ -\frac{v}{l}\tan\kappa\sin^2\beta \\ -\frac{v}{l}\tan\kappa\cos\beta\sin\beta \end{bmatrix}$$
$$\underset{(x_b,y_b,z_b)}{\boldsymbol{\alpha}} = \begin{bmatrix} \dot{\sigma}_2 \\ -\frac{v}{l}\tan\kappa\sin(2\beta)\sigma_2 \\ -\frac{v}{l}\tan\kappa\cos(2\beta)\sigma_2 \end{bmatrix} \tag{11}$$

are the angular velocity and acceleration of the board given in the board fixed (x_b, y_b, z_b) coordinate system, respectively, and the mass moment of inertia matrix of the board is

$$\underset{(x_b,y_b,z_b)}{\mathbf{J}_b} = \begin{bmatrix} J_1 & 0 & 0 \\ 0 & J_2 & 0 \\ 0 & 0 & J_3 \end{bmatrix} \tag{12}$$

With these, the energy of acceleration can be expressed as

$$\mathcal{A} = \frac{hv}{l^2}m\tan\kappa\cos\varphi(al\sigma_2\cos\beta + v\sin\beta(l - h\tan\kappa\sin\beta\sin\varphi))\dot{\sigma}_1 + \frac{v^2}{l^2}\tan^2\kappa(J_3 - J_2)\sin^3\beta\cos\beta\dot{\sigma}_2 + \frac{1}{2}mh^2\dot{\sigma}_1^2 + \frac{1}{2}J_1\dot{\sigma}_2^2 + \cdots \tag{13}$$

where the terms that do not depend on the pseudo-acceleration are not computed here since they will disappear after derivation in the Gibbs–Appell equation (6).

The pseudoforce can be determined from the virtual power of the active forces, which here relates to the torques produced by the controller and the spring and the damper in the suspension system and to the gravitational force

$$\delta P = mgh\sin\varphi\delta\sigma_1 + M_{PD}(\delta\sigma_2 - \delta\sigma_1) - (k_t\beta + k_d\sigma_2)\delta\sigma_2 \tag{14}$$

where notation δ refers to virtual quantities.

Thus, based on Eq. (6), the equations of motion assume the forms

$$\begin{aligned}
\dot{\sigma}_1 &= \frac{g}{h}\sin\varphi - \frac{av}{hl}\tan\kappa\sigma_2\cos\beta\cos\varphi - \frac{v^2}{hl}\tan\kappa\sin\beta\cos\varphi + \frac{v^2}{l^2}\tan^2\kappa\sin^2\beta\sin\varphi\cos\varphi - \frac{1}{h^2m}(d\sigma_1(t-\tau) + p\varphi(t-\tau)) \\
\dot{\sigma}_2 &= \frac{p\varphi(t-\tau) + d\sigma_1(t-\tau)}{J_1} - \frac{k_t\beta + k_d\sigma_2}{J_1} + \frac{J_2 - J_3}{J_1}\frac{v^2}{l^2}\tan^2\kappa\sin^3\beta\cos\beta \\
\dot{\varphi} &= \sigma_1 \\
\dot{\beta} &= \sigma_2 \\
\dot{x} &= v\cos\psi - \frac{av\tan\kappa\sin\beta\sin\psi}{l} \\
\dot{y} &= v\sin\psi - \frac{av\tan\kappa\sin\beta\cos\psi}{l} \\
\dot{\psi} &= -\frac{v\tan\kappa\sin\beta}{l}
\end{aligned} \tag{15}$$

Note, that x, y, and ψ are cyclic coordinates, so only the first four equations of Eq. (15) describe the so-called essential motion; these are needed for the stability analysis.

4 Stability of the Rectilinear Motion

In this section, the linear stability of the rectilinear motion is investigated. First, we take the linearized equations of motion around this stationary solution with respect to small perturbations in σ_1, σ_2, φ, and β. This leads to

$$\dot{\mathbf{X}}(t) = \mathbf{A}\cdot\mathbf{X}(t) + \mathbf{B}\cdot\mathbf{X}(t-\tau) \tag{16}$$

where

$$\mathbf{A} = \begin{bmatrix} 0 & -\frac{av}{hl}\tan\kappa & \frac{g}{h} & -\frac{v^2}{hl}\tan\kappa \\ 0 & -\frac{k_d}{J_1} & 0 & -\frac{k_t}{J_1} \\ 1 & 0 & 0 & 0 \\ 0 & 1 & 0 & 0 \end{bmatrix},$$
$$\mathbf{X}(t) = \begin{bmatrix} \sigma_1(t) \\ \sigma_2(t) \\ \varphi(t) \\ \beta(t) \end{bmatrix} \quad \text{and} \quad \mathbf{B} = \begin{bmatrix} -\frac{1}{mh^2}d & 0 & -\frac{1}{mh^2}p & 0 \\ \frac{1}{J_1}d & 0 & \frac{1}{J_1}p & 0 \\ 0 & 0 & 0 & 0 \\ 0 & 0 & 0 & 0 \end{bmatrix} \tag{17}$$

Note, that the two principle mass moments of inertia J_2 and J_3 of the board have no effect on the dynamics close to the rectilinear motion.

The stability of this linear system can be determined by the real part of the roots of the corresponding characteristic equation

$$\left(\lambda^2 + \frac{k_d}{J_1}\lambda + \frac{k_t}{J_1}\right)\left(\lambda^2 - \frac{g}{h} + \left(\frac{d}{mh^2}\lambda + \frac{p}{mh^2}\right)e^{-\lambda\tau}\right) + \frac{v}{l}\left(\frac{a}{h}\lambda + \frac{v}{h}\right)\tan\kappa\left(\frac{d}{J_1}\lambda + \frac{p}{J_1}\right)e^{-\lambda\tau} = 0 \tag{18}$$

with characteristic exponent λ. Although, a characteristic equation of a delayed system has infinitely many complex roots [23], the investigated equilibrium is asymptotically stable if and only if all of the real parts of these roots are negative. The limit of stability corresponds to the case when the characteristic roots are located on the imaginary axis for a set of specific values of system parameters.

One can distinguish basically two different types of stability boundaries. The first relates to the saddle-node (SN) bifurcation, which occurs when both the real and the imaginary parts of the characteristic root are zeros; the second refers to Hopf bifurcation, when the characteristic roots are pure imaginary.

SN bifurcation occurs if $\lambda_{SN} = 0$ satisfies the characteristic Eq. (18), namely, if

$$\frac{k_t}{J_1}\left(-\frac{g}{h} + \frac{p}{h^2m}\right) + \frac{p}{J_1}\frac{v^2}{hl}\tan\kappa = 0 \tag{19}$$

equation leads to the possibly critical proportional gain p_{SN}

$$p_{SN} = \frac{g}{h}\frac{k_t}{\frac{v^2}{hl}\tan\kappa + \frac{k_t}{mh^2}} \tag{20}$$

The critical proportional and differential gains in case of Hopf bifurcation can be determined by the D-subdivision method. In this case, the critical characteristic exponent is a pure imaginary number ($\lambda_H = \pm i\omega$, $\omega \in \mathbb{R}^+$) which can be substituted back into the characteristic equation. Taking the real and imaginary parts of this complex equation, the critical control gains can be expressed as

$$p_{\mathrm{H}} = p_1 \frac{(p_2 + p_3)\cos(\tau\omega) - p_4 \sin(\tau\omega)}{p_5 + l(2p_2 + p_3)} \tag{21}$$

$$d_{\mathrm{H}} = p_1 \frac{(p_2 + p_3)\sin(\tau\omega) + p_4 \cos(\tau\omega)}{\omega(p_5 + l(2p_2 + p_3))} \tag{22}$$

where

$$\begin{aligned} p_1 &= mlh(g + h\omega^2) \\ p_2 &= mhv \tan\kappa(\omega^2(ak_{\mathrm{d}} - J_1 v) + k_{\mathrm{t}} v) \\ p_3 &= l((k_{\mathrm{t}} - J_1\omega^2)^2 + k_{\mathrm{d}}^2\omega^2) \\ p_4 &= mhv \tan\kappa(aJ_1\omega^2 - ak_{\mathrm{t}} + k_{\mathrm{d}} v)\omega \\ p_5 &= (mhv \tan\kappa)^2(a^2\omega^2 + v^2) \end{aligned} \tag{23}$$

Based on the stability boundaries given in Eqs. (20)–(22), a linear stability chart of the rectilinear motion can be constructed. The SN bifurcation is represented with a vertical line in the p–d parameter plane (see any panel of Fig. 2). Only control gains from the right-hand side of this SN bifurcation line can correspond to stable rectilinear motion.

The Hopf bifurcation curve, also called dynamical stability boundary is more complicated. It starts like the stability boundary in case of the PD-controlled inverted pendulum (see in Refs. [12] and [15]), but before it spirals outward uniformly, it forms an enclosed loop, which contains the origin ($p = 0$, $d = 0$). In a special case, when the damping of the skateboard (k_{d}) is zero, this stability boundary goes throw the origin (see details in Ref. [9]). The loop of the dynamic stability boundary has a major effect on the structure of the stable domain in the p–d plane, namely, it can be proved that only the inner part of this loop can be stable.

One can observe in Fig. 2 that the possibly stable closed loop rotates counterclockwise around the origin as the time delay increases, which implies that the stable domain can vanish and reappear as the delay varies. The panels of Fig. 2 also show the effect of the damping coefficient k_{d} in the suspension system, which increases from top to bottom. One can observe that the higher the damping coefficient is, the larger the closed loop is. In cases when the closed loop bounds the actual stable regime, the rectilinear motion can loose its stability with higher frequencies, corresponding to the board's natural frequency. This vibration frequency is high at low damping coefficients due to the relatively small mass moment of inertia of the board J_1.

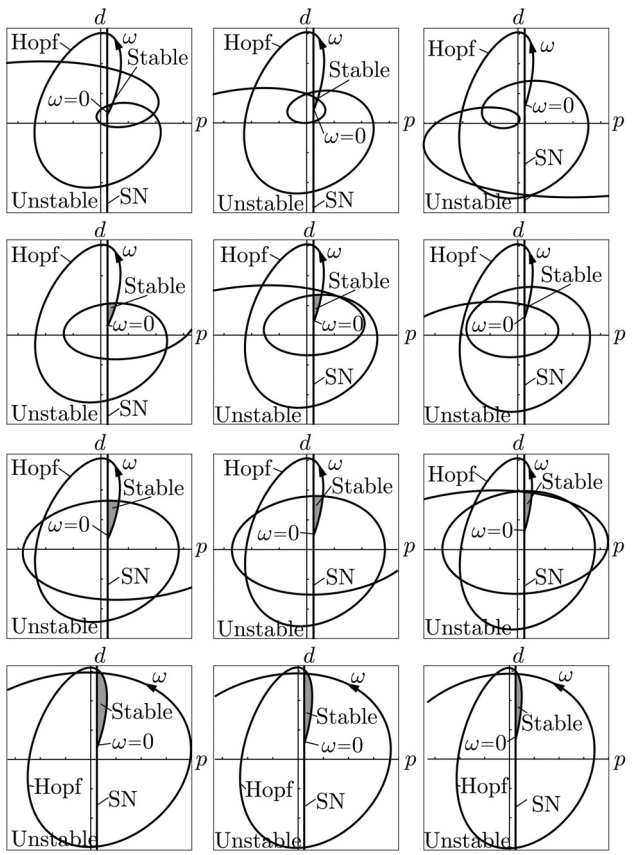

Fig. 2 Qualitative structure of the stability charts in the *p–d* plane, where the shaded domains indicate the stable regimes. The time delay τ increases from left to right, and the damping coefficient k_d increases from top to bottom.

5 Critical Reflex Delay

The effect of the time delay τ is intricate. It can only be investigated numerically, but before the presentation of this, we are going to give a sufficient condition for the delay. This condition can be developed by the examination of the starting point of the Hopf stability boundary curve. This always starts on the SN line, but if it goes to the left-hand side first, then, the stable domain cannot exist. This leads to the ultimate critical time delay $\tau_{\mathrm{cr,u}}$, practically, if the reflex delay of the skater is larger than this value, the investigated equilibrium is unstable. The sufficient condition can be determined as

$$\left.\frac{d^2 p_{\mathrm{H}}}{d\omega^2}\right|_{\omega=0} > 0 \tag{24}$$

since the first derivative at $\omega = 0$ is still zero. The condition can be formed as a second-order inequality in terms of the delay

$$-\frac{t_2}{t_1}\tau^2 + \frac{t_3}{t_1^2}\tau + \frac{t_4}{t_1^3} > 0 \tag{25}$$

where

$$\begin{aligned} t_1 &= hmv^2 l \tan\kappa + k_{\mathrm{t}} \\ t_2 &= mghlk_{\mathrm{t}} \\ t_3 &= 2gh^2 lm^2 v \tan\kappa(ak_{\mathrm{t}} - k_{\mathrm{d}} v) \\ t_4 &= 2h^2 lm(gmv^2 \tan\kappa(hmv \tan\kappa(ak_{\mathrm{d}} - J_1 v) + k_{\mathrm{d}}^2 l) \\ &\quad + mv \tan\kappa(hmv \tan\kappa(hv^2 - a^2 g) - gl(ak_{\mathrm{d}} + J_1 v))k_{\mathrm{t}} \\ &\quad + 2hlmv^2 \tan\kappa k_{\mathrm{t}}^2 + l^2 k_{\mathrm{t}}^3) \end{aligned} \tag{26}$$

Without further mathematical investigations, we plot the ultimate critical delay (see Fig. 3) using the realistic numerical values of Table 1. In Fig. 3, the continuous and dashed lines refer to the cases when the skater stands ahead ($a = 0.1$ m) and behind ($a = -0.1$ m) the center of the board, respectively.

Although the ultimate critical time delay can be expressed analytically from Eq. (25), the arising expressions are complex. At zero and infinite longitudinal speeds, the critical time delay is independent from the standing position a

$$\begin{aligned} \tau_{\mathrm{cr,u}}^{v\to 0} &= \frac{\sqrt{2}}{\omega_{\mathrm{s}}} \\ \tau_{\mathrm{cr,u}}^{v\to\infty} &= -\frac{2\zeta_{\mathrm{b}}}{\omega_{\mathrm{b}}} + \sqrt{\left(\frac{2\zeta_{\mathrm{b}}}{\omega_{\mathrm{b}}}\right)^2 + 2\left(\frac{1}{\omega_{\mathrm{b}}^2} + \frac{1}{\omega_{\mathrm{s}}^2}\right)} \end{aligned} \tag{27}$$

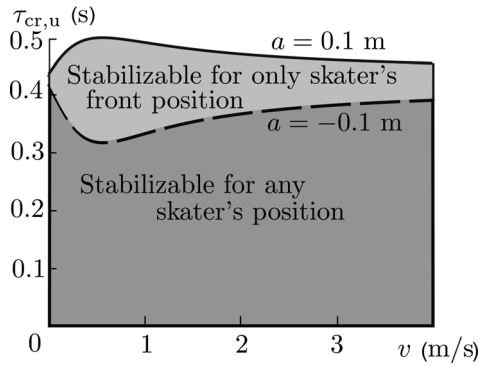

Fig. 3 Effect of the longitudinal speed on the ultimate time delay; continuous line refers to the fore standing ($a = 0.1$ m), while the dashed line refers to the back standing ($a = -0.1$ m)

Table 1 Parameters of the skater–board system

h (m)	m (kg)	a (m)	τ (s)
0.85	75	± 0.1	0.24
k_t (N·m/rad)	l (m)	κ (deg)	J_1 (kg m^2)
100	0.3937	63	6.642×10^{-3}

where ζ_b and ω_b are the damping ratio and the natural angular frequency of the skateboard, respectively. The notation ω_s refers to the natural angular frequency of the pendulum of length h. These parameters can be formulated as

$$\zeta_b = \frac{1}{2\omega_b}\frac{k_d}{J_1}, \quad \omega_b = \sqrt{\frac{k_t}{J_1}}, \quad \text{and} \quad \omega_s = \sqrt{\frac{g}{h}} \tag{28}$$

Note, that the ultimate reflex time at zero speed $\tau_{cr,u}^{v\to 0}$ is identical with the critical time delay for simple human balancing [12]. The ultimate time delay at infinitely high speed is slightly greater than the standing one. The difference is small if the relative damping ratio (ζ_b) is small, and the natural angular frequency of the board is much higher than the skater's one ($\omega_b \gg \omega_s$).

Besides these analytical results, the critical time delay can be determined numerically. The existence of the stable regime in Fig. 4 was determined in the plane of the longitudinal speed and the time delay with the help of the semidiscretization method [24]. In the shaded domains, there exists sufficient p, d control gains, for which the rectilinear motion is stable. The continuous lines refer to the real stabilizability boundaries, while the dashed lines stand for the analytically determined ultimate critical time delay. As the boundary of the ultimate critical time delay depends on the position of the skater, the stability boundaries also do. Thus, in the upper panels, stabilizability charts belong to the case where the skater stands behind the center of the board ($a = -0.1$ m), while in the lower panels one can find the standing ahead case ($a = 0.1$ m).

One can observe in Fig. 4, that the ultimate critical time delay does not give a necessary and sufficient condition for the existence of stable rectilinear motion. The shaded domains are always below the ultimate value. Moreover, at low damping ratio, ζ_b, there are time delay ranges, for which the rectilinear motion is unstable. At high damping ratio, these unstable ranges disappear, and the critical time delay can be approximated by the analytically determined ultimate time delay well.

6 Required Control Gains

The existence of stable control gains does not ensure stability automatically; appropriate selection of the gains is necessary. In Fig. 5, stable control gain domains are plotted for several longitudinal speeds, v, and damping ratios, ζ_b, using the parameters of Table 1. The stable domains are shaded for the damping ratio $\zeta_b = 0.36$. The arising closed loop cuts off some domains, at sufficiently small damping ratios, from the possibly stable regular D-shaped stability boundary. The higher the damping ratio is, the larger the stable domain is, as it was expected from the structure of the Hopf stability boundary curves. However, extremely large damping ratio cannot increase the stable domain further, while it may provide more difficult handling of the skateboard, i.e., it

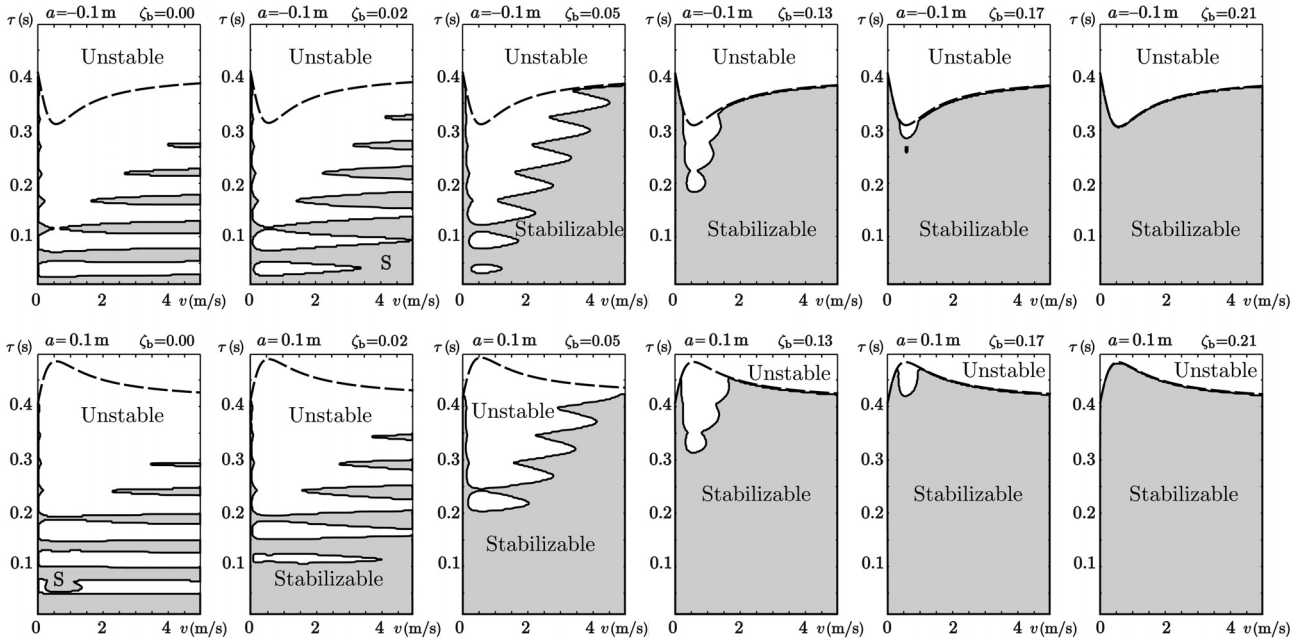

Fig. 4 Effect of the longitudinal speed and the damping ratio on the critical time delay; continuous lines stand for stability boundaries, dashed lines do for ultimate critical time delay, and the shaded domain indicates *p–d* stabilizable domains, while the white domains are unstable. The upper row belongs to the standing behind and the row below belongs to the standing ahead.

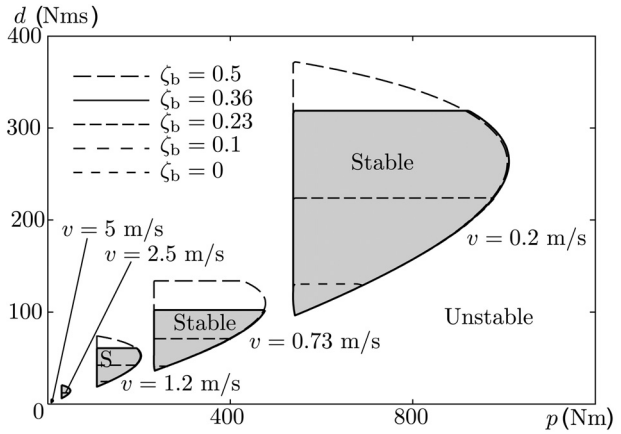

Fig. 5 Effect of the speed and the damping ratio on the required control gains

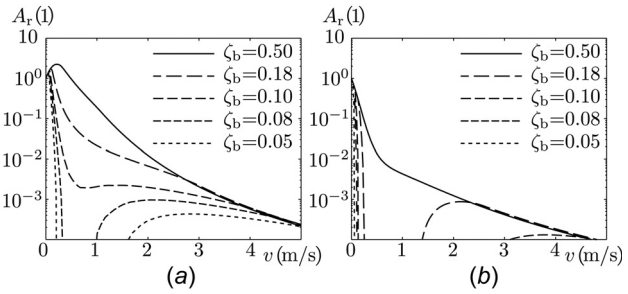

Fig. 6 Effect of the speed and the damping ratio on the area of stable domain in *p–d* plane; panel (*a*) belongs to the standing ahead case ($a = 0.1$ m), while panel (*b*) refers to the standing behind one ($a = -0.1$ m)

requires larger control effort to tilt the board and make cornering maneuvers.

The speed has basically two different effects on the stable domain in the p, d parameter plane; as the speed changes, the location and the size of the stable regimes also change. Thus, the skater's proportional and differential gains must be tuned as the longitudinal speed varies; this effect makes skateboarding even more challenging.

The reduction of the stable parameter domain can explain the loss of stability at high speeds although one can observe more stabilizable domains (v, τ) in Fig. 4 at higher speeds. Namely, the higher the speed is, the smaller the domain of the appropriate p, d control gains is. This makes the sensitivity for the control gains greater. The area of the stable domain is illustrated in Fig. 6 relative to the area of the stable domain at zero speed. If the area of the stable domain is zero, the rectilinear motion cannot be stabilized by linear PD controller with the time delay $\tau = 0.24$ s. These domains belong to an unstable regime of the corresponding panel in Fig. 4.

7 Conclusion

A mechanical model of the skateboard–skater system was constructed, in which the effect of the human balancing was taken into account by a linear delayed PD controller. The linear stability of the rectilinear motion of the skateboard was analyzed, and stability charts were composed with special attention to the effects of the reflex time and the longitudinal speed apart from the effect of the damping coefficient of the skateboard suspension system.

An upper limit was given for the critical time delay, which approximate the necessary and sufficient stability condition for the time delay well at relatively high damping ratio. The sensitivity of the system with respect to the longitudinal position of the skater was also shown. The advantages of the fore standing are clear at high damping ratios and especially at low speeds. But, at low damping ratios, the skater also has opportunity to make the system stabilizable by means of the variation of the longitudinal position on the board. For example, the variation of the time delay due to the modified concentration level of the skater can be balanced by the appropriately chosen position of the skater.

The presented model can also explain the loss of stability at high speeds. Although, appropriate control gains exist at high speeds by which the rectilinear motion is stable, stability is not guaranteed, because the chance of choosing satisfactory control gains is smaller for higher speeds. The sensitivity with respect to the control gains is large; small error in the chosen control gains can lead to loss of stability. There is another issue that makes skateboarding at high speed difficult. Namely, small control gains can be applied only, which results close to zero torque, and this enlarges the effect of the deadzones of the human control system. In case of human stick balancing, these effects are identified in Ref. [15] as the sources of microchaotic and transient-chaotic vibrations around linearly unstable equilibrium with large surviving times.

Acknowledgment

This research was partly supported by the Janos Bolyai Research Scholarship of the Hungarian Academy of Sciences and by the Hungarian National Science Foundation under Grant No. OTKA PD105442.

References

[1] Kane, T. R., and Levinson, D. A., 2005, *Dynamics, Theory and Applications*, The Internet-First University Press, Ithaca, New York.
[2] Hubbard, M., 1979, "Lateral Dynamics and Stability of the Skateboard," ASME J. Appl. Mech., **46**(4), pp. 931–936.
[3] Wisse, M., and Schwab, A. L., 2005, "Skateboards, Bicycles, and Three-Dimensional Biped Walking Machines: Velocity-Dependent Stability by Means of Lean-to-Yaw Coupling," Int. J. Rob. Res., **24**(6), pp. 417–429.
[4] Kooijman, J. D. G., Meijaard, J. P., Papadopoulos, J. M., Ruina, A., and Schwab, A. L., 2011, "A Bicycle Can Be Self-Stable Without Gyroscopic or Caster Effects," Science, **332**(6027), pp. 339–342.
[5] Kremnev, A., and Kuleshov, A., 2007, "Nonlinear Dynamics and Stability of a Simplified Skateboard Model," *The Engineering of Sport 7*, Vol. 1, pp. 135–142.
[6] Ispolov, Y., and Smolnikov, B., 1996, "Skateboard Dynamics," Comput. Methods Appl. Mech. Eng., **131**(3–4), pp. 327–333.
[7] Hubbard, M., 1980, "Human Control of the Skateboard," J. Biomech., **13**(9), pp. 745–754.
[8] Rosatello, M., Dion, J.-L., Renaud, F., and Garibaldi, L., 2015, "The Skateboard Speed Wobble," ASME Paper No. DETC2015-47326.
[9] Varszegi, B., Takacs, D., and Stepan, G., 2015, "Skateboard: A Human Controlled Non-Holonomic System," ASME Paper No. DETC2015-47512.
[10] Varszegi, B., Takacs, D., Stepan, G., and Hogan, S. J., 2016, "Stabilizing Skateboard Speed-Wobble With Reflex Delay," J. R. Soc. Interface, **13**(121), p. 20160345.
[11] Milton, J. G., Solodkin, A., Hluštík, P., and Small, S. L., 2007, "The Mind of Expert Motor Performance Is Cool and Focused," NeuroImage, **35**(2), pp. 804–813.
[12] Stepan, G., 2009, "Delay Effects in the Human Sensory System During Balancing," Philos. Trans. R. Soc., A, **367**(1891), pp. 1195–1212.
[13] Chagdes, J. R., Rietdyk, S., Jeffrey, M. H., Howard, N. Z., and Raman, A., 2013, "Dynamic Stability of a Human Standing on a Balance Board," J. Biomech., **46**(15), pp. 2593–2602.
[14] Chagdes, J. R., Haddad, J. M., Rietdyk, S., Zelaznik, H. N., and Raman, A., 2015, "Understanding the Role of Time-Delay on Maintaining Upright Stance on Rotational Balance Boards," ASME Paper No. DETC2015-47857.
[15] Insperger, T., and Milton, J. G., 2014, "Sensory Uncertainty and Stick Balancing at the Fingertip," Biol. Cybern., **108**(1), pp. 85–101.
[16] McRuer, D. T., Weir, D. H., Jex, H. R., Magdeleno, R. E., and Allen, E. W., 1975, "Measurement of Driver-Vehicle Multiloop Response Properties With a Single Disturbance Input," IEEE Trans. Syst., Man, Cybern., **SMC-5**(5), pp. 490–497.
[17] Gantmacher, F., 1975, *Lectures in Analytical Mechanics*, MIR Publisher, Moscow, Russia.
[18] Peterka, R. J., 2002, "Sensorimotor Integration in Human Postural Control," J. Neurophysiol., **88**(3), pp. 1097–1118.

[19] Maurer, C., and Peterka, R. J., 2004, "A New Interpretation of Spontaneous Sway Measures Based on a Simple Model of Human Postural Control," J. Neurophysiol., **93**(1), pp. 189–200.
[20] Vette, A. H., Masani, K., Nakazawa, K., and Popovic, M. R., 2010, "Neural-Mechanical Feedback Control Scheme Generates Physiological Ankle Torque Fluctuation During Quiet Stance," IEEE Trans. Neural Syst. Rehabil. Eng., **18**(1), pp. 86–95.
[21] Kremnev, A. V., and Kuleshov, A. S., 2008, "Dynamics and Simulation of the Simplest Model of a Skateboard," European Nonlinear Dynamics Conference 2008 (ENOC-2008), Saint Petersburg, Russia, June 30–July 4.
[22] Varszegi, B., Takacs, D., Stepan, G., and Hogan, S. J., 2014, "Balancing of the Skateboard With Reflex Delay," Eighth EUROMECH Nonlinear Dynamics Conference (ENOC2014), Vienna, Austria, July 6–11.
[23] Stepan, G., 1989, *Retarded Dynamical Systems: Stability and Characteristic Functions*, Longman Scientific and Technical Co-Published With Wiley, New York.
[24] Insperger, T., and Stépán, G., 2011, *Semi-Discretization for Time-Delay Systems: Stability and Engineering Applications*, Vol. 178, Springer Science and Business Media, Berlin.